Volume 10
Number 6
June 2025
Pages 1187–1432

# Reaction Chemistry & Engineering

Linking fundamental chemistry and engineering to create scalable, efficient processes

rsc.li/reaction-engineering

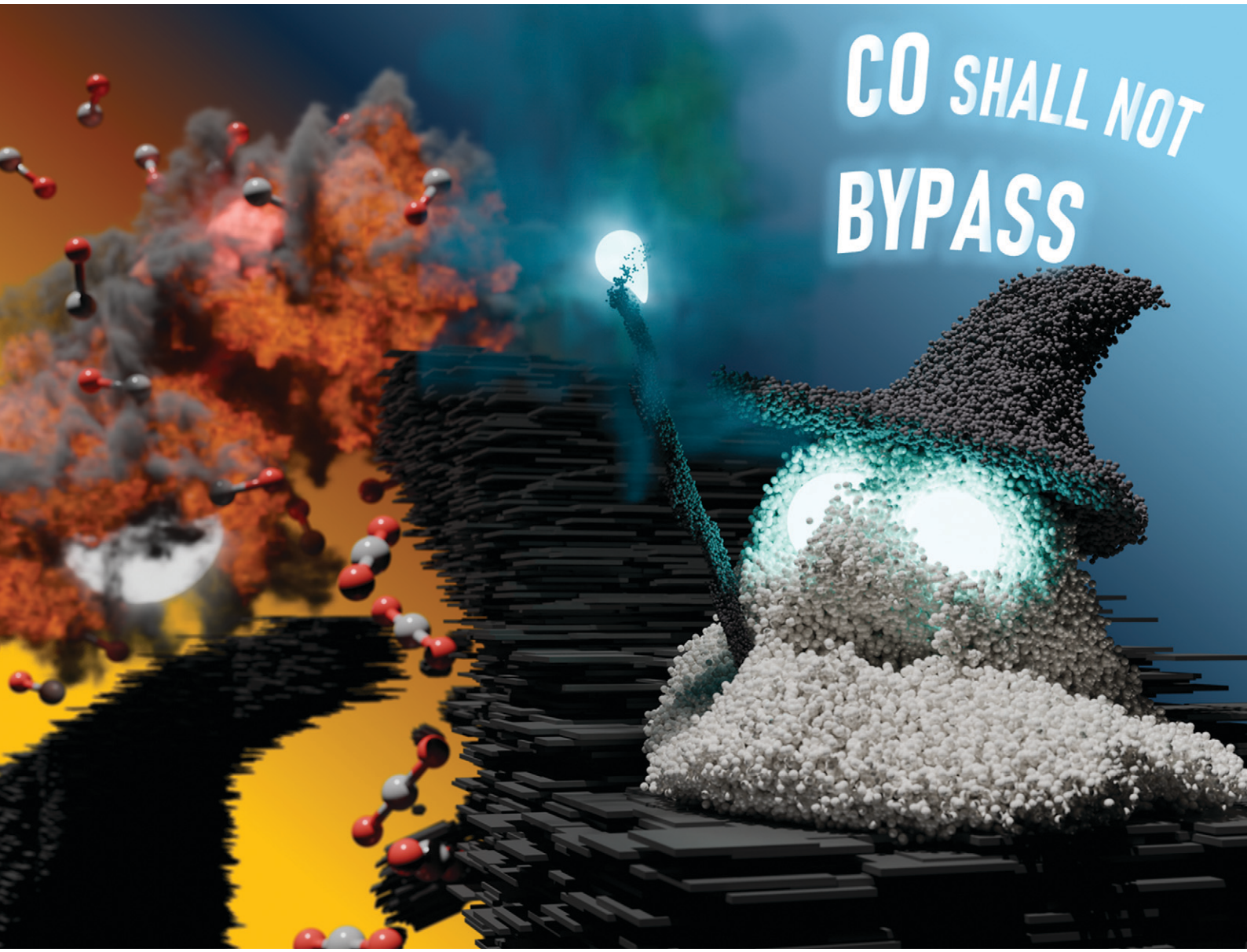


ISSN 2058-9883

ROYAL SOCIETY OF CHEMISTRY

**PAPER**

Anna Zimina, Jan-Dierk Grunwaldt *et al.*
Role of powders and coatings for relating catalytic activity and structure of Pt in emission control catalysis

Reaction Chemistry & Engineering

ROYAL SOCIETY OF CHEMISTRY

PAPER

View Article Online
View Journal | View Issue



Cite this: *React. Chem. Eng.*, 2025, **10**, 1233

# Role of powders and coatings for relating catalytic activity and structure of Pt in emission control catalysis†

Samuel Struzek, [a] Tim Delrieux, [a] Florian Maurer, [a] Danielle Santos Gonçalves, ‡[b] Sarina-Lena Heck, [a] Linda Klag, [a] Joachim Czechowsky, [a] Anna Zimina *[ab] and Jan-Dierk Grunwaldt *[ab]

Packed powder beds and coatings are two relevant forms of catalysts, applied in industrial heterogeneous catalysis and multiple fundamental studies including *operando* spectroscopy. Both types have their individual advantages and disadvantages in regard to the performance and characterisation causing some complexity in the resulting flow patterns, possible temperature inhomogeneities in the reactor and the dynamic evolution of chemical state of the noble metal during the reaction along the catalytic bed. The well-known CO oxidation reaction over $Pt/Al_2O_3$ catalysts was used in this study to uncover the influence of the gas phase compositions and the temperature on the evolution of the electronic structure of Pt for powdered and coated catalysts at comparable length scales. Advanced *operando* investigations were used to demonstrate the influence of spatial gradients in the gas phase for washcoats in contrast to packed powder beds. Additionally, transient gradients in the chemical state of Pt, which occurred more pronounced for packed powder beds than for coated monoliths were followed and traced back to heat and mass transfer effects. Finally, the catalytic activity can be linked to the temperature distributions for both types of samples. These findings will be valuable for planning and evaluating future combinations of spectroscopic and catalytic experiments on industrially relevant systems.

Received 28th May 2024,
Accepted 19th March 2025

DOI: 10.1039/d4re00262h

rsc.li/reaction-engineering



## 1 Introduction

Effective and stable catalysts are essential for the chemical industry, in the circular economy and in environmental chemistry.[1,2] Depending on the requirements of the process, different structured catalysts are applied. Whereas in the lab sieved catalyst powders and coated catalysts are applied, in industrial applications both extrudates including shell-impregnated pellets and coated substrates are used.[3] The choice of the kind of structured catalyst is important, because accessibility of the active sites limited by internal and external mass transfer processes and stability in regard to the process conditions must be assessed.[4,5] Thus, for each application, the type of catalyst has to be individually chosen to achieve the highest process efficiency while simultaneously being easy to manufacture. Challenges like pressure drop at high space velocities as well as internal mass and heat transfer limitations can be minimized by using thin washcoats.[6] For this reason thin catalytic layers on *e.g.* monolithic or annular reactors are advantageous and often utilized for performing fast kinetic studies on heterogeneous catalysts in various fields of catalysis like emission control, steam reforming and methanation.[7,8]

*In-situ* spectroscopic studies have been conducted on catalysts of different shapes, for instance on packed powder bed reactors using X-ray spectroscopic and scattering techniques as well as Raman spectroscopy,[9,10] on thin catalyst coatings using fluorescence X-ray spectroscopy, surface X-ray diffraction[3,11–14] and transmission electron spectroscopy[15] and on crystalline surfaces (*e.g.* by XRD[16]). However, external and internal mass transfer limitations can still occur for non-ideal reactor geometries[17] and have already been visualized in a two dimensional manner by the planar laser induced fluorescence (PLIF) method.[18,19] Possibilities to minimize external mass transfer limitations by increasing the Reynolds number for monolithic samples which leads to a turbulent gas flow[20] and therefore prohibits gas from bypassing the monolith, or by

[a] *Institute for Chemical Technology and Polymer Chemistry (ITCP), Karlsruher Institute of Technology (KIT), Engesserstrasse 18, 76131 Karlsruhe, Germany. E-mail: anna.zimina@kit.edu, grunwaldt@kit.edu*
[b] *Institute of Catalysis Research and Technology (IKFT), Karlsruher Institute of Technology (KIT), Hermann-von-Helmholtz-Platz 1, 76344 Eggenstein-Leopoldshafen, Germany*

† Electronic supplementary information (ESI) available: XANES LCA fits; details on the estimations of: Reynolds number, Thiele modulus, Weisz modulus, Damköhler number, Mears criterium and pressure drop. See DOI: **https://doi.org/10.1039/d4re00262h**

‡ Current affiliation: Brazilian Synchrotron Light Laboratory (LNLS), National Center for Research in Energy and Materials (CNPEM), 13083-100, Campinas, São Paulo, Brazil.

changing the reactor geometry to a packed powder bed reactor have been explored. Packed beds have the advantage that the reactor concept is rather flexible and can easily be down-scaled, making them attractive for catalytic tests in laboratories and for advanced *in-situ*/*operando* characterization methods like X-ray absorption spectroscopy (XAS) which provides insights into the chemical state of active noble metal with a time scale of minutes and a spacial resolution in the mm range. XAS experiments require a suitable reactor design, so that the structure–performance relations can be revealed.[21] Besides mass transfer limitations the catalyst shape affects the catalytic behaviour on multiple dimensions in form of pressure drop formation in the reactor,[22] complex flow patterns depending on geometry and temperature[23,24] and particularly for exothermic reactions in the appearance of strong temperature gradients along the reactor.[25] The reaction temperature directly influences the rate and (local) changes in the temperature can lead to significant differences in the chemical state of the active metal as it might reduce/oxidize during the reaction.[26] Donazzi *et al.*[27] showed that the temperature of a monolithic cordierite honeycomb surface measured by optical pyrometry is similar to that of the gas-phase. Therefore, active noble metal species and the gas phase exhibit a very similar temperature for thin coatings. In contrast, packed powder beds may exhibit strong temperature gradients throughout the catalyst bed cross-section (from the centre to the surface of the packed bed).[28] As pyrometry measurements of packed powder beds reveal only the temperature on the surface, the temperature within the packed powder beds can be determined with a thin thermocouple, like realized in the SpaciPro testing setup which is used for monolithic honeycombs[29,30] or with a compact profile reactor (Reacnostics GmbH) developed by Horn *et al.*[31–34] Catalytic coatings and packed powder beds both have their individual advantages which makes them mandatory for specific measurement techniques. However, transfer of knowledge between these systems is challenging as secondary effects such as temperature or mass transfer have strong influences on the reaction rates. The scope of this paper is to compare the catalytic performance of typical reactors with power beds and structured catalysts. Hereby, the catalytic performance and the structure of the catalyst are linked to the catalyst shape. For this purpose we report the temperature gradients, the different chemical states of Pt and the gas phase composition for three types of catalysts: honeycombs with thin coating layers, a chip with a thick coated layer and packed powder beds. As model reaction, the CO oxidation under lean conditions with a $Pt/Al_2O_3$ catalyst is used since this reaction is well understood and frequently used as benchmark in literature.

# 2 Experimental

## 2.1 Catalyst preparation

The catalyst was prepared by an automated incipient wetness impregnation utilizing a SYNTHESIZER CATIMPREG platform (Chemspeed Technologies AG).[35] Tetraamine platinum nitrate (Alfa Aesar/Strem Chemicals) was used as precursor. For the support commercially available γ-alumina (Puralox TH 100/150, Sasol Germany GmbH) was used. The platinum loading was confirmed by ICP-OES measurements. The noble metal particle size was determined by transmission electron microscopy (TEM). The $Pt/Al_2O_3$ catalyst exhibited a Pt loading of 1.88 ± 0.10 wt% and an average noble metal particle size of 2.0 ± 0.9 nm.

## 2.2 Catalyst shapes

**2.2.1 Packed powder bed catalysts.** The catalyst was used in different ways: As a powder, the catalyst was first pressed for 5 min with 6.6 kg $mm^{-2}$ and afterwards mortared and sieved with a sieve fraction of 100–200 μm. For diluted powders, pure $\gamma$-$Al_2O_3$ was added to the catalyst powder while mortaring prior to the pressing and sieving. **Sieved powder catalyst bed 1:** the catalyst was diluted to 0.38 wt%. 210 mg of the diluted $Pt/Al_2O_3$ catalyst were filled into a quartz capillary with an inner diameter of 4 mm. The catalyst was diluted to obtain a similar catalyst bed length at the same amount of Pt in comparison to the 9-channel monolith. The catalyst powder bed length was 20 mm and the powder was held in place by quartz wool. Sieved powder catalyst bed 1 was used for spatially resolved CO conversion investigations. **Sieved powder catalyst bed 2:** the catalyst was diluted to 0.27 wt% in order to prevent hot-spot formation. 5.7 mg of the diluted $Pt/Al_2O_3$ catalyst were filled into a quartz capillary with an inner diameter of 1.5 mm. The catalyst bed length was 6 mm and the powder was held in place by quartz wool. Sieved powder catalyst bed 2 was used for spatially resolved Pt $L_3$-edge XAS *operando* investigations of the catalysts chemical state. Due to the different dilutions of the $Pt/Al_2O_3$ powders with $\gamma$-$Al_2O_3$ the weight hourly space velocities (WHSV), defined by the total gas flow divided by the amount of Platinum are presented for all reactions instead of the gas hourly space velocities (GSHV), which do not consider the different Pt loadings of the catalysts.

**2.2.2 Washcoated catalysts.** For the catalyst in a coated form a suspension was prepared by adding 56.9 mg of commercial aluminium hydroxide (Dispersal P2, Sasol Germany GmbH) to 569 mg of the catalyst followed by mortaring. Then 10 ml of distilled water were added, followed by ball milling at 500 rpm for 5 min. Afterwards, nitric acid was added under constant stirring until the pH-value reached 3. This suspension was then applied to different substrates. **Coated catalyst 1:** the coating was conducted by dip-coating the cylindrical monolith (diameter 24 mm, length 24 mm, channel size 1.04 × 1.04 × 24 $mm^3$) under constant stirring, followed by blowing off excess liquid at room temperature and drying the sample at 300 °C for about one minute. These steps were repeated until 1.54 g of the catalyst was deposited on the monolith, followed by a calcination at 550 °C in static air. A 3 × 3 channel piece of the monolith containing 800 μg of Pt with an estimated layer thickness of about 100 μm was cut out and placed inside a quartz capillary with an inner diameter of 5 mm. The monolith was held in place by glass wool. The coated catalyst 1 was used for spatially resolved conversion measurements. **Coated catalyst 2:** the coating was conducted

 

by dip-coating the cylindrical monolith (diameter 24 mm, length 24 mm, channel size 1.04 × 1.04 × 24 $mm^3$) under constant stirring, followed by blowing off excess liquid at room temperature and drying the sample at 300 °C for about one minute. These steps were repeated until 0.36 g of the catalyst was deposited on the monolith followed by a calcination at 550 °C in static air. One wall of a channel was cut out, shortened to a length of 7.5 mm and placed inside a quartz capillary with an inner diameter of 1.5 mm. This monolith wall sample contained 2.45 μg of Pt with a resulting washcoat thickness of well below 100 μm. The monolith was held in place by quartz wool. The coated catalyst 2 was used for spatially resolved Pt $L_3$-edge XAS *operando* investigations of the chemical state of the catalyst. **Coated catalyst 3:** the coating was conducted by drop-casting without spin-coating on a chip (material: Rubalit 708S, $L \times W \times H$ = 25.4 × 4.1 × 0.63 $mm^3$, company: CeramTec) followed by drying at 75 °C. Hereby, only about 11 mm of the chips length were coated (Fig. 1c). This procedure was repeated several times until 12.7 mg of the catalyst was deposited. Afterwards, the chip was calcined for 5 hours in static air. The chip with an estimated washcoat thickness of 700 μm was mounted inside a continuous flow cell.[36] The coated catalyst 3 was used for Pt $L_3$-edge XAS *operando* investigations of the chemical state of the catalyst.

### 2.3 Characterization methods

For all experiments, gases were dosed by mass-flow controlers (MFC, Bronkhorst Deutschland Nord GmbH) through the reactor and the gas conversions were determined by mass-spectrometry (Omnistar™, Pfeiffer Vacuum GmbH), Fourier-transform infra-red spectroscopy (FTIR, Gasmet, MKS instruments), non-dispersive infrared spectrometry (company ABB) and micro gas chromatography (μGC, Inficon Fusion, Inficon GmbH). The Pt/$Al_2O_3$ catalyst was investigated using *operando* techniques including spatially resolved gas phase profiling, spatially resolved analysis of the chemical state and distribution of the temperature *via* infrared thermography.

**Spatially resolved gas phase profiling.** For the spatially resolved gas phase profiling a compact profile reactor (Reacnostics GmbH) was used.[31] The reactor consists of a large metal body which is internally heated by resistive heating. A small tubular quartz reactor (inner diameter 4–5 mm) which contains the catalyst is placed inside. Through the middle of the catalyst, along the catalyst bed a 75 μm thick hollow metal capillary for gas sampling with 4 orifices that are close to each other was positioned. The orifices of this metal capillary can draw a tiny amount of gas in, which then flows to the gas analytics. By moving the catalyst in respect to the orifices of the metal capillary, the gas phase can be probed in a spatially resolved manner. For the investigation of the monolith, a 3 × 3 channel chunk of the monolith (coated catalyst 1) was cut out and placed inside of a quartz capillary with an inner diameter of 5 mm. The sampling metal capillary went hereby through the central channel. The monolith was held in place by glass wool. The

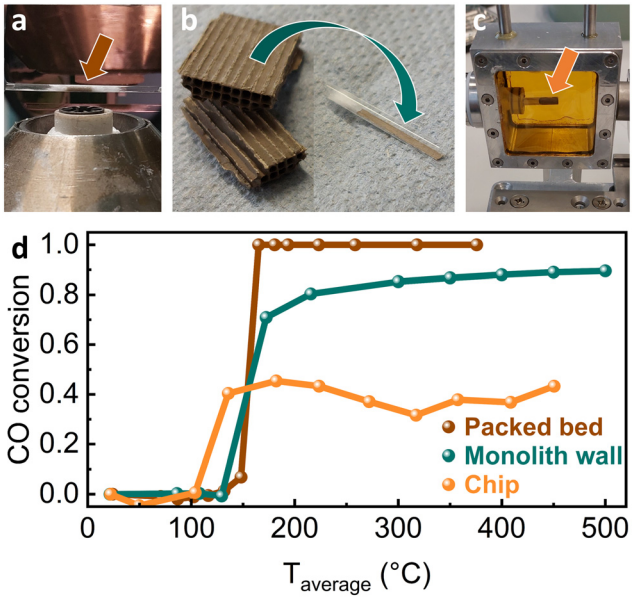


e

| | | | | External MTL | | | Internal MTL | | |
|---|---|---|---|---|---|---|---|---|---|
| | T (°C) | WHSV ($l h^{-1} g^{-1}$) | Δp (mbar) | Re | $Da_{II}$ | Mears | Φ | η | Ψ |
| Powder | 150 | 2.0E+05 | 5 | 8 | 0.002 | 0.30 | 0.09 | 1.00 | 0.0027 |
| Monolith | 150 | 1.2E+06 | | 169 | 2.5 | | 0.08 | 1.00 | |
| Chip | 150 | 1.2E+04 | | 1 | 94 | | 2.56 | 0.39 | |

**Fig. 1** Different forms of the Pt/$Al_2O_3$ catalyst used for activity tests, IR and XAS characterisations: (a) packed powder bed inside of a quartz capillary micro-reactor placed above a hot air gas blower; (b) monolith wall coated with a catalyst slurry inside a quartz capillary which is placed on top of a hot air gas blower; (c) coated chip with resistive heating patterns on its uncoated backside inside a continuous flow cell. (d) Total CO conversions (dosed: 1000 ppm CO, 10% $O_2$ in inert gas) at different average temperatures for the three different forms of catalysts. (e) Dimensionless numbers for the three different catalyst shapes. Average catalyst temperature ($T$), weight hourly space velocity (WHSV), pressure drop ($\Delta p$), Reynolds number (Re). Criteria for external mass transfer limitations (MTL): Damköhler number II ($Da_{II}$) and Mears criterion. Criteria for internal mass transfer limitations: Thiele modulus ($\Phi$), effectiveness factor $\eta$ and Weisz modulus ($\Psi$). Details on the estimations are provided in the ESI.†

sampling metal capillary was connected to a mass spectrometer (MS) and a micro gas chromatograph (μGC). The CO and $CO_2$ concentrations were obtained from the measurements of the μGC. For the investigation of the packed powder bed catalyst, a dilution with further γ-$Al_2O_3$ was necessary (sieved powder catalyst bed 1) to achieve a reasonable comparison to the monolith with a similar catalyst bed length. The concentration profiles were determined by a MS while a Fourier transform infra-red (FTIR) spectrometer monitored the concentrations behind the end of the reactor. For both, the monolith and the packed powder bed, the gas flow was set to 50 ml/min in total, containing 1000 ppm CO, 10 vol% $O_2$ and a mixture of the inert gases $N_2$ and He for the rest. The weight hourly space velocity (WHSV) for both samples was 3700 L $h^{-1}$ $g^{-1}$ (litres of gas per hour and grams of platinum).

**Spatially resolved analysis of the oxidation state and structure.** The chemical state of platinum was determined by

X-ray absorption spectroscopy (XAS) at the Pt $L_3$ edge (11.564 keV) at the CAT-ACT beamline[37] of the KIT Light Source (Karlsruhe, Germany). A Si and a Rh mirror together with a Si(111) double crystal monochromator were used for the experiments. The beamsize ($W \times H$) was 1.0 × 1.0 $mm^2$ for the packed powder bed, 1.5 × 1.5 $mm^2$ for the coated monolith wall and 1.5 × 2.0 $mm^2$ for the coated chip. The absorption spectra were recorded in transmission mode with gas ionisation chambers (OKEN Ltd, Japan) and simultaneously in fluorescence mode using a SDD solid state detector (1E-Vortex, Hitachi High-Tech America, Inc.). Three different forms of the same catalyst were investigated by XAS: a powder inside a quartz capillary (sieved powder catalyst bed 2, 2.0 × $10^5$ L $h^{-1}$ $g^{-1}$), a coated wall cut out of a monolith inside a quartz capillary (coated catalyst 2, 1.2 × $10^6$ L $h^{-1}$ $g^{-1}$) and a coated chip inside of a continuous flow cell (coated catalyst 3, 1.2 × $10^4$ L $h^{-1}$ $g^{-1}$). While the gas flow was identical across the experiments, the amount of catalyst varied due to experimental limitations resulting in different WHSVs. The capillaries with the powdered catalyst and with the coated monolith wall were placed 5 mm above the hot-air gas blower for the heating. The chip which was placed inside a 32 ml continuous flow cell with an X-ray transparent Kapton window on the back side and an infrared radiation and X-ray transparent polyamide window at the front side was heated by Ag/Pd resistive heating structures on the backside of the chip.

Due to the low amounts of noble metal loading, X-ray fluorescence data (Pt $L\alpha_{1,2}$ lines) were used for the evaluation of the XAS spectra instead of transmission data. The X-ray absorption near edge structure (XANES) data was calibrated, background subtracted, normalized and smoothed (boxcar average, kernel size 7) using the Demeter software package Version 0.9.26.[38] For the linear combination analysis transmission XANES spectra from a Pt foil ($Pt^0$) and an oxidized $Pt/Al_2O_3$ pellet ($Pt^{4+}$) were chosen as standards. It is known from literature[39] that $Pt^{2+}$ also plays an important role for CO oxidation. However, identification of $Pt^{2+}$ using conventional XANES is not unambiguously possible since a linear combination of $Pt^0$ and $Pt^{4+}$ can easily be mistaken for $Pt^{2+}$. For this reason, only the most reduced and oxidized Pt species were used as references for the LCA.

**Temperature distribution.** For the infrared thermography (IRT) measurements an ImageIR camera (InfraTec GmbH) was used. The thermograms were collected using the IRBIS 3 Software (InfraTec GmbH). The average temperatures of the catalysts during the XAS measurements were calculated from the IR measurements, using in-house developed scripts based on the software IgorPro version 8.0.

# 3 Results and discussion

## 3.1 CO conversion over different catalyst shapes and reaction cell geometries

For comparing the chemical state of Pt for different catalyst shapes, *operando* XAS measurements were conducted on a packed powder bed and a coated monolith wall in a quartz reactor as well as on a coated chip in a high flow cell (Fig. 1a–c). The chemical state of Pt is dependent on the gas atmosphere which changes with the temperature due to catalytic conversion. The corresponding CO conversion curves are shown in Fig. 1d. For the experiments a lean gas mixture of 1000 ppm CO and 10% $O_2$ in inert gas was dosed. Due to the different geometries and amounts of catalyst, the weight hourly space velocities $\mathrm{WHSV} = \frac{\mathrm{d}V_{\mathrm{gas}}}{\mathrm{d}t \cdot m_{\mathrm{Pt}}}$ were different for each experiment. Here $\frac{\mathrm{d}V_{\mathrm{gas}}}{\mathrm{d}t}$ is the total gas flow and $m_{\mathrm{Pt}}$ - the mass of Platinum. The corresponding WHSVs are included in Fig. 1, which shows the total conversion of CO as a function of the average sample temperature for the three catalytic systems.

The packed powder bed showed a steep conversion profile with 50% conversion at around $T_{50}$ = 155 °C. The powder catalyst was the only one of the 3 geometries with principally 100% conversion. In regard to the pressure drop, the packed bed was estimated to exhibit a difference in pressure $\Delta p_b$ along its whole length $L_b$ in the range of 0–10 mbar (see ESI† for estimation), which is well within the recommended range for catalytic experiments:[40] $\frac{\Delta p_b}{L_b} < 0.2\frac{p_{tot}}{L_b}$. Note that the pressure drop can be expected to be even lower for the washcoated catalysts than for the packed powder bed. Furthermore, the reactor diameter was 10 times the particle diameter which implies, that wall effects can be neglected.[40] In the kinetic regime (CO conversion $X_{CO} < 20\%$) at 150 °C (see Fig. 1e), the packed powder bed exhibited a Damköhler number II of $Da_{II} \approx 0.002$. Such a small value below the threshold of approximately 0.02, indicates that the catalyst is unlikely to suffer from external mass transfer limitations (MTL).[41] Furthermore, the Thiele ($\Phi$) and the Weisz ($\Psi$) moduli were 0.09 and 0.003 respectively, indicating also the absence of internal mass transfer limitations. Note that in general, for a Thiele modulus below 0.3 and a Weisz modulus below 0.1 for first order reactions, the catalyst is considered to be unaffected by internal mass transfer limitations.[42] In regard to the flow profile, the Reynolds number was approximately 8, which suggests a laminar flow profile. Note that turbulent flow for packed beds with spherical particles occurs for Reynolds numbers above $10^2$ (*cf.* ref. 43), for cylindrical reactors without powders above 2300 (*cf.* ref. 20) and for overflown plates in the order of magnitude $10^5$.

The coated monolith wall (Fig. 1d) exhibited the same light-off temperature ($T_{50}$ = 155 °C) as the packed powder bed. However, it was not able to reach 100% CO conversion, even at 500 °C. According to literature, the relatively shallow temperature dependent CO conversion increase could suggest internal mass transfer limitations.[44] However, the Thiele modulus ($\Phi$) was 0.08, indicating that the catalyst was unlikely to be influenced by internal mass transfer limitations. Since the Damköhler number II was, with a value of 2.5, relatively high, external mass transfer limitations can not be excluded. Therefore, the shallow conversion increase above 200 °C could originate from external mass transfer

 

limitations. Furthermore, the fact that the catalyst did not reach full conversion may even suggest a gas bypass.[17,45]

The chip within the continuous flow cell (Fig. 1c) showed a maximum CO conversion of about 40%. The Damköhler number II was estimated to be 94, suggesting the presence of external mass transfer limitations. The washcoat on the chip was, with a calculated thickness of 700 μm much thicker than that on the monolith wall (21 μm) or the particle size of the packed powder bed (150 ± 50 μm). Therefore, internal mass transfer limitations are more likely to occur. The Thiele modulus ($\Phi$) was estimated to be 2.6, which is above the threshold value of 0.3 above which internal mass transfer limitations are generally expected to be present.[42] Note furthermore that due to the large dead volume of the reactor, a bypass of gas can also not be excluded. Although for XAS such unfavourable geometries for *in-situ* cells can be circumvented, we find various cells like this in literature, *e.g.* for surface X-ray diffraction,[46] *operando* transmission electron microscopy[47] and *in-situ* X-ray photoelectron spectroscopy.[48]

### 3.2 Structural evolution of Pt along the catalyst bed

In a next step the effect of CO-conversion in the various spectroscopic reaction cells on the chemical state of the catalyst is discussed as the local CO and oxygen concentration have a direct influence on the state of the catalyst. This can lead to spatial gradients of the chemical noble metal state along the catalyst bed.[49] Furthermore, the bulk sensitivity of XAS[50] can result in diminished changes of the chemical noble metal state if the catalyst is subject to internal mass transfer limitations (*e.g.* for thick washcoats).[5] In this study, the electronic state of Pt was investigated during the CO oxidation reaction not only *operando* and in a spatially resolved manner but also for different catalyst shapes as shown in Fig. 2 and 3. The chemical state of the catalyst was evaluated by linear combination analysis (LCA) with oxidized Pt (obtained from measurement of oxidized reference sample) and reduced Pt (obtained from measurement of a Pt foil) as LCA references. Pt with adsorbed CO was not used as a reference species since it is hardly distinguishable from metallic Pt with standard XANES.

Due to the initial high oxidation state of the samples at room temperature (Fig. 2a), the Langmuir–Hinshelwood mechanism[51] may be suppressed due to the lack of available metallic Pt sites, where CO and oxygen can adsorb. Above room temperature the catalyst started to reduce likely due to small amounts of CO that reacted with oxygen from the oxidized Pt particles, desorbed and left behind metallic sites that are available for CO adsorption. When the lowest oxidation state possible for the system was reached, the conversion increased and the catalyst started to re-oxidize. This re-oxidation which can be seen in Fig. 2a at temperatures above 150 °C, is a direct consequence of the higher oxygen to CO ratio in the gas. This is sketched in Fig. 2b and has already been observed before in

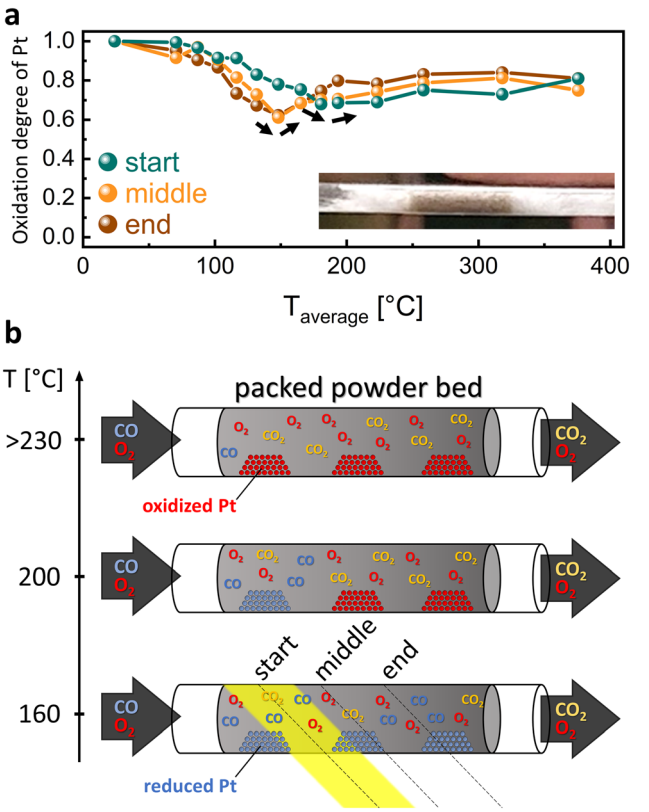


**Fig. 2** a) Temperature dependent evolution of the Pt oxidation state at different position for the packed powder bed shown in Fig. 1. The standard error of the LCA is ±2%. Black arrows indicate the temperatures where the re-oxidation occurs. The corresponding temperature dependent total CO conversion is shown in Fig. 1d. b) Sketch of the gas composition and the chemical state of Pt along the packed bed for different temperatures. The dashed lines indicate where the X-rays (depicted exemplary for one position in yellow) penetrate the packed powder bed during the spatially resolved investigation.

literature.[49,52] At 160 °C the catalyst achieved full CO conversion along the whole catalyst bed and CO was still present at all positions along the catalyst bed. With increasing temperature the front where CO was absent and the catalyst was exposed only to $CO_2$ and $O_2$ moved upstream and led to a re-oxidation of the catalyst at different positions of the bed. For temperatures above 230 °C, CO became already completely converted at the very start of the catalyst bed and the whole length of the bed exhibited a high oxidation state. Note that since the X-rays hit the sample under an incident angle of 45° which was chosen for obtaining a sufficient but unsaturated fluorescence signal (90° between incoming beam and detector[53]), the information obtained from the XAS measurements was an average of a larger area. This is sketched for the start position at 160 °C in Fig. 2b.

The temperature dependent evolution of the chemical state of Pt for the coated monolith wall and the coated chip from Fig. 1b and c are displayed in Fig. 3. The general behaviour of the monolithic sample was similar to that of the packed powder bed, but the spatial gradient seen for the packed bed (Fig. 2a) was absent. The re-oxidation

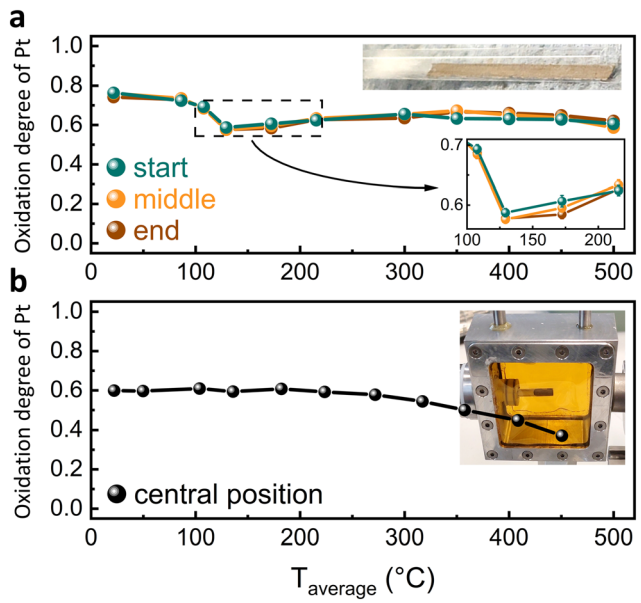


Fig. 3 Temperature dependent evolution of the platinum oxidation state for the a) monolith wall and b) chip, shown in Fig. 1. The standard error of the LCA is ±2%. The corresponding temperature dependent total CO conversions are shown in Fig. 1d.

occurred for all positions at the same temperature (130 °C) due to the higher WHSV and external mass transfer limitations ($Da_{II}$ = 2.5), so that CO was always present at every position along the catalyst. In contrast to the packed powder bed, there was no clear front in the gas phase beyond which CO was absent.

The evolution of the oxidation state of Pt on the chip is shown in Fig. 3b. The XAS measurements were conducted at the central position of the chip. Below 200 °C no visible changes in the oxidation state of Pt were observed. Due to the large thickness of the coating most of the Pt on the chip is more likely to suffer from internal mass transfer limitations ($\Phi$ = 2.6) which limited the CO oxidation reaction more to the surface of the washcoat. Therefore, XAS which is a bulk sensitive technique showed hardly any changes in the oxidation state of Pt, since changes would mostly occur at the outer surface. For temperatures above 300 °C all three catalysts (packed powder bed, coated monolith wall, coated chip) showed a reduction behaviour. This reduction can be explained by the increase in empty Pt sites at elevated temperatures due to the decreasing residence time of adsorbates on Pt.[4]

In summary, external mass transfer limitations which we observed for the washcoats, but not for the packed powder bed were shown to lead to diminished gradients in the chemical state of the catalyst. For the thick washcoat, internal mass transfer limitations allowed only the outer surface of the catalyst to participate in the reaction. Therefore, changes in the chemical state of the catalyst in the surface layer were barely observed by bulk sensitive XAS. As a consequence, when the chemical state of the catalyst is to be compared between laboratory studies and industrial scale in a global as well as in a spatially resolved manner, the WHSV as well as the mass transfer have to be considered (*e.g.* for VOC oxidation[17,45]).

### 3.3 Evaluation of temperature distribution along the catalytic bed

For the heating of catalysts, compromises between heating efficiency and feasibility have often to be made, especially when it comes to *operando* XAS measurements. A hot air blower is for example an often used and easy to handle way to heat packed powder beds. Typically heat shields of X-ray transparent materials (*e.g.* Kapton) are utilized in order to provide a better temperature homogeneity. This is however not possible, when the temperature is observed by Infra-red thermography since the IR radiation cannot penetrate the heat shield. Depending on the experimental requirements (*e.g.* isothermicity, heating rate) optimized heating methods (*e.g.* split furnace) can be applied. But such heating methods are also not universally applicable and fail for experiments where fluorescence or diffraction is recorded (*e.g.* HERFD-XAS, fluorescence XAS, XRD). In this study, the packed powder bed and the monolith wall have been heated by a hot air blower which is displayed in Fig. 1a. The coated chip exhibited resistive heating structures, printed on its backside. Since the catalytic activity and the chemical state are strongly dependent on the temperature as can be seen in Fig. 1d, 2a and 3 the temperature distributions over the catalyst bed for the different catalytic systems should be known in detail. Therefore, infrared thermography measurements were conducted on a packed powder bed and a monolith wall inside quartz reactors above a hot air gas blower as well as on a coated chip in a continuous flow cell which was heated by resistive heating structures printed on its backside (see Fig. 1a–c). The results of the temperature analysis are displayed in Fig. 4. Note that in contrast to the chip and the packed bed, the temperature of the coated monolith wall was not measured during the light-off experiments displayed in Fig. 1d but separately on another, identical sample.

Even for the closest packed powder bed in a capillary the sample does not reach the temperature set in the temperature controller of the hot air gas blower.[54] The temperature distributions in Fig. 4 show the temperature profiles of the marked area for selected average temperatures. The distributions that are depicted in orange and which have similar average temperatures were obtained at a temperature set point of 170 °C for the packed powder bed, 225 °C for the monolith wall and 150 °C for the chip. Since the packed powder bed and the monolith wall exhibited similar average temperatures, even though the set point of the hot air gas blower was 55 °C higher for the monolith wall, it can be concluded that the heating of the monolith wall was much less efficient, likely due to the low contact of the monolith wall with the capillary reactor. The chip was heated directly by resistive heating structures printed onto the chips backside and exhibited the narrowest temperature distribution. For all three samples no shielding was applied for reducing gradients in

 

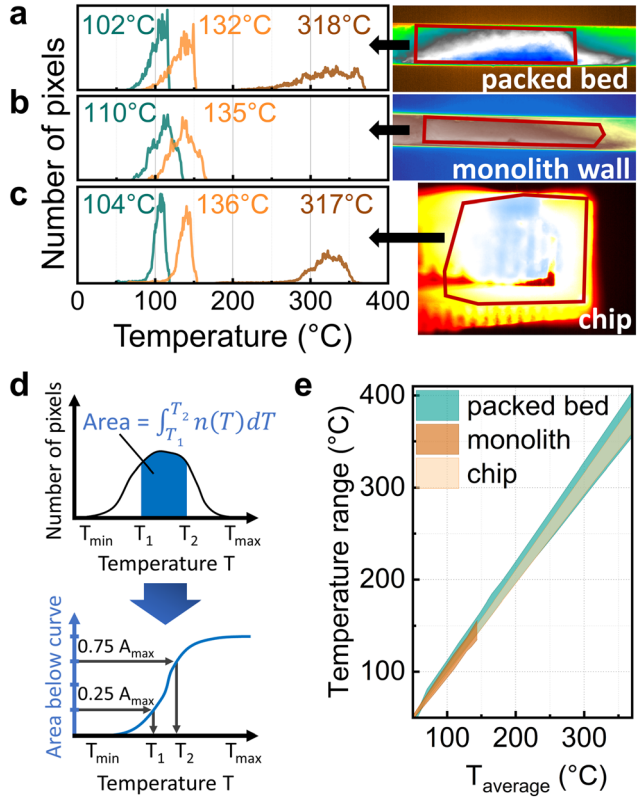


**Fig. 4** Selected temperature histograms (left) and the typical thermograms with the marked in red analysed areas (right): (a) packed powder bed, displayed in Fig. 1a; (b) coated monolith wall, similar to the one displayed in Fig. 1b; (c) coated chip, displayed in Fig. 1c. The average temperatures are indicated. The gas inlet is on the left side. (d) Definition of the temperature range $T_1 \leq T \leq T_2$ based on analysis of thermograms. (e) Temperature distribution for different catalyst forms at different average temperatures.

temperature and therefore these measurements are extreme cases. For the packed bed and the monolith in the quartz reactors the hottest areas were those closest to the hot air gas blower nozzle and the temperature decreased strongly in horizontal and vertical direction. In case of the chip the temperature decreased at the positions far from the electrodes due to the low thermal conductivities of the coating and the chip material. The temperature ranges $T_1 \leq T \leq T_2$ are evaluated for every temperature for all three samples and displayed in Fig. 4e. Ranges were chosen by weighting the number of pixels within the marked area with their respective temperature, which is depicted as the area beneath the curve in Fig. 4d, followed by selecting the temperatures $T_1/T_2$ below/above which 25% of the temperature weighted amount of pixels lay. The range was chosen in this way, so that small areas with strong deviations in temperature from the majority of the sample, do not influence the temperature range. From Fig. 4e it can be seen that the sample variation of temperature increased for all samples with increasing average temperatures. The monolith wall showed the broadest temperature distribution followed by the packed powder bed. The narrowest distribution was obtained for the coated chip. The broad temperature distribution of the monolith wall was likely due to the limited contact with the quartz reactor while the high homogeneity of the chip can be attributed to the evenly distributed resistive heating structure that is in direct contact with the chip.

The broader temperature distribution of the coated monolith wall could explain the light-off behaviour shown in Fig. 1d. Here, the packed bed and the monolith wall exhibited CO oxidation insets at roughly the same temperatures. Due to the WHSV of the monolith wall being 6 times higher than that of the packed powder bed, the monolith walls light-off is expected to occur at higher temperatures than that of the packed bed. However, since the monolith wall exhibited a larger temperature distribution (note that usually a heat shield or similar efforts are taken to prevent this), some parts of the washcoat had a higher temperature in comparison to the packed powder bed for the same average sample temperature. According to the Arrhenius equation the catalytic activity roughly doubles with every additional 10 degrees in temperature.[4] Therefore, in case of the monolith wall, the hotter parts of the catalyst that exhibited higher temperatures than those of the packed bed would contribute much more to the catalytic activity. This could explain, why no difference in light-off temperature was observed between the powder packed bed and the monolith wall despite the difference in WHSV.

The temperature distribution had a noticeable influence on the catalytic activity. Resistive heating structures showed a narrower temperature distribution than the heating with a hot air gas blower, which makes them superior in terms of exploiting the largest amount of noble metals due to the strong activity dependence on the temperature. The broad temperature distribution of the packed bed and the monolith wall heated by hot air blower indicate the need for improved heating methods like *e.g.* heating coils in close contact to the reactor[55] or inductive heating.[56,57] Furthermore, applying a cap with Kapton windows above the hot air blower and around the quartz reactor is known to improve the temperature homogeneity. Alternatively, for XAS investigations on weakly absorbing samples, a split furnace can be utilized[31] which generally exhibits a more homogeneous temperature profile.

### 3.4 Spatially resolved CO conversion study

A direct comparison of the CO conversion was performed for the $Pt/Al_2O_3$ catalyst in packed powder bed form and as a coated layer on a 3 × 3 channel monolith. The catalysts inside the quartz reactors were mounted inside the Reacnostics compact profile reactor. Both samples exhibited a similar catalyst length, the same amount of platinum and an identical WHSV. Also for these catalysts, the pressure drop and the reactor diameter in ratio to the sieve fraction were well within the recommended limits (see ESI†).[40]

Fig. 5a displays the CO conversion profiles along the catalyst packed powder bed. For all temperatures the CO

conversion increased linearly along the catalyst bed. Such a linear conversion behaviour can also be found in literature for catalyst foams in a similar reactor.[31] Note that the position uncertainty with this setup was always ±2 mm. Fig. 5b shows the conversion profiles for the 3 × 3 channel monolith, which increase linearly along the monolith channel within the first half of the catalyst. In the second half of the catalyst, the conversion per length decreases. In literature, a non-linear behaviour of a $Pt/Al_2O_3$ coated monolith has also been observed for the same gas composition at a 16 times higher WHSV.[49] Hereby, the sampling technique was however different, which affects the gas phase.[58] For the coated monolith wall the CO conversion rate deviated from the linear behaviour towards the end of the reactor (Fig. 5b). As indicated by the Damköhler numbers II and the Thiele moduli in Fig. 5c, none of the two catalysts is likely to suffer from external or internal mass transfer limitations since $Da_{II}$ and $\Phi$ are small. Therefore, mass transfer limitations are unlikely to be the cause for this non-linear conversion behaviour. It is claimed in literature[58] that the introduction of a gas sampling capillary, which reduces the cross section of the channel leads to a lower gas velocity within that channel. As a consequence, the gas that went through the central channel, which was the probed channel, exhibited a higher CO conversion due to the lower WHSV in comparison to the gas which went through the other channels. The gas with the higher velocity from the other channels mixed with that of the probed channel at the end of the catalyst *via* gas diffusion as depicted in Fig. 5d. The mixture of the central channel gas with gas that experienced less conversion led then to a decrease in measured CO conversion towards the end of the central channel of the monolith. Note, that there is also the possibility that, due to the laminar flow profile ($Re(T) < 10$) some of the CO completely bypassed the monolith as suggested within Fig. 5d. For a direct comparison of the two catalyst forms the conversion rates normalized to the amount of platinum were calculated for different temperatures. Due to the non-linear behaviour of the conversion observed for the monolith, only the first half of the catalyst bed was used for the calculation of the normalized conversion rates and the results are depicted in Fig. 6.

The normalized to the amount of platinum conversion rates of CO at different reactor temperatures for the packed powder bed and the monolith are shown in Fig. 6. The measurement of the packed powder bed was conducted at 117 °C instead of 123 °C, where both samples would have been comparable. This lower temperature of 117 °C was chosen because the packed powder bed exhibited already full conversion at 123 °C. This full conversion can occur due to the heat release during the exothermic reaction when the catalyst powder is not sufficiently diluted. The temperature of 99 °C where CO conversion is in the range of 10% to 20% (kinetic regime) is best suited for a comparison of the two

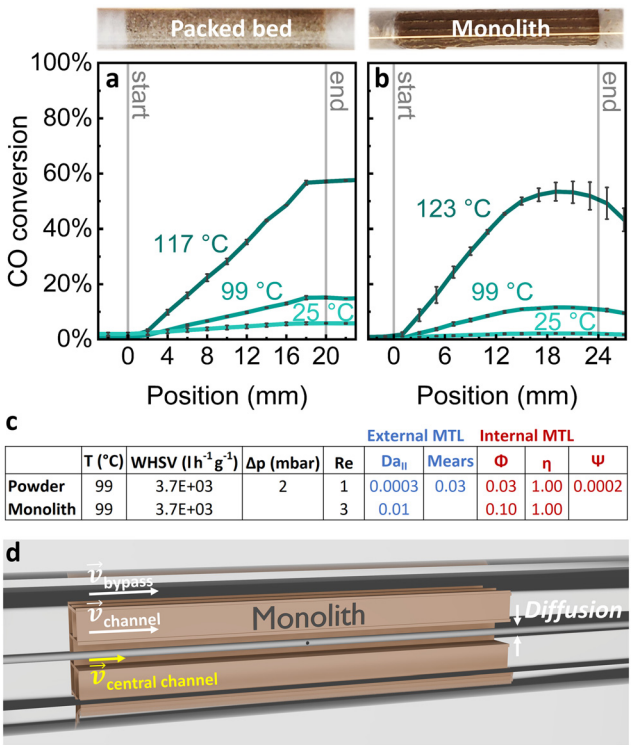


c

| | T (°C) | WHSV ($l h^{-1} g^{-1}$) | Δp (mbar) | Re | External MTL $Da_{II}$ | External MTL Mears | Internal MTL Φ | Internal MTL η | Internal MTL Ψ |
|---|---|---|---|---|---|---|---|---|---|
| Powder | 99 | 3.7E+03 | 2 | 1 | 0.0003 | 0.03 | 0.03 | 1.00 | 0.0002 |
| Monolith | 99 | 3.7E+03 | | 3 | 0.01 | | 0.10 | 1.00 | |




**Fig. 5** Spatially resolved, temperature dependent CO conversion profiles of $Pt/Al_2O_3$ catalysts: (a) diluted $Pt/Al_2O_3$ packed powder bed (sieved powder catalyst bed 1) inside a quartz reactor with an inner diameter of 4 mm; (b) 3 × 3 channel monolith with a $Pt/Al_2O_3$ coating (coated catalyst 1) inside a quartz reactor with an inner diameter of 5 mm. Gas feed: 1000 ppm CO and 10% $O_2$. (c) Dimensionless numbers for the two different catalyst shapes. Average catalyst temperature ($T$), weight hourly space velocity (WHSV), pressure drop ($\Delta p$), Reynolds number (Re). Criteria for external mass transfer limitations (MTL): Damköhler number II ($Da_{II}$) and Mears criterion. Criteria for internal mass transfer limitations: Thiele modulus ($\Phi$), effectiveness factor $\eta$ and Weisz modulus ($\Psi$). Details on the estimations are provided in the ESI.† (d) Sketch of the monolith within the quartz reactor: gas velocity vectors show the gas flow behaviour, gas feed from left.

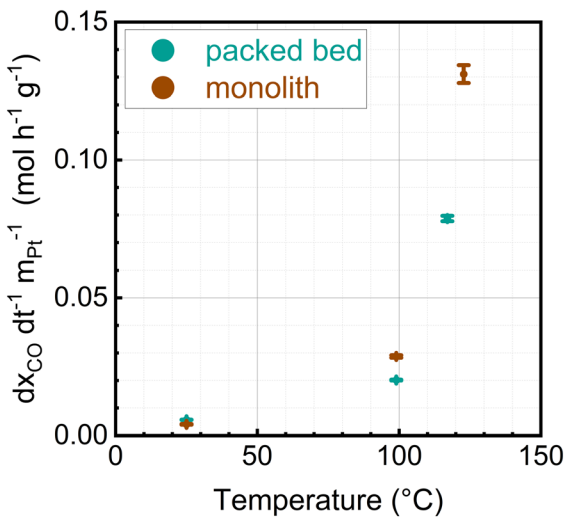


**Fig. 6** CO conversion rates (integrated over the first half of the bed) normalized to the amount of platinum in the packed powder bed and coated monolith. The calculations are given in the ESI.†

systems because the signal to noise ratio is sufficient (in contrast to 25 °C) and the slope in the conversion-temperature curve is much shallower in contrast to 117 °C. At 99 °C the normalized reaction rate of the monolith was 50% higher than that of the packed powder bed. Because the temperature profile within the packed powder bed, measured with a thermocouple, was very homogeneous and showed only a temperature increase of 0.2 °C along the whole catalyst bed, any influences of temperature hot spots which can occur for exothermic reactions[26,59] could be excluded here. The monolith showed a higher normalized reaction rate, likely because of the change in gas velocity the probed monolith channel experienced because of the influence of the sampling capillary. Due to the generally lower WHSV of the probed channel the normalized reaction rate of the monolith shown in Fig. 6 is overestimated. That is, without a gas sampling probe, the normalized reaction rate would be lower.

Spatially resolved conversion measurements with the capillary sampling technique on a coated honeycomb showed non-linear behaviours in contrast to the packed powder bed which exhibited linear profiles along the catalytic bed. Therefore packed powder beds appear to be more suitable for this type of testing.

## 4 Conclusions

In this study coatings with different thicknesses as well as packed powder beds were investigated with the intent of unravelling similarities, differences and limitations of these catalyst shapes for *operando* spectroscopic studies. For this purpose a state-of-the-art $Pt/Al_2O_3$ catalyst prepared with incipient wetness impregnation was investigated during CO oxidation under lean conditions as example reaction. The occurrence of internal and external mass transfer limitations and their influence on the oxidation state of the catalyst were evaluated.

In the kinetic regime at 150 °C, the packed powder bed which was not subject to any kind of mass transfer limitations, showed spatial gradients in the oxidation state of Pt during the reaction, due to the presence and absence of CO along the catalyst bed. At this temperature, the coated monolithic sample, which suffered from dead volume and external but likely not from internal mass transfer limitations showed no spatial gradient in the oxidation state of Pt. We attribute this to a homogeneous CO distribution in the gas phase along the catalyst bed. For a thick coating layer, which was subject to internal and external mass transfer limitations at 150 °C, changes in the chemical state of Pt were diminished. The bulk probing XAS technique is therefore not applicable to systems, where changes occur only close to the surface of the catalyst. These findings reveal, that internal and external mass transfer limitations have to be considered, if spectroscopic data obtained on different catalyst shapes are to be compared.

Furthermore, the temperature profiles of the different catalytic shapes were analysed. The chip with the printed resistive heating structure showed the best temperature homogeneity due to the uniform heating. The monolith wall and the packed powder bed were heated by a hot air blower which led to vertical and horizontal temperature gradients in the absence of shielding and broadened the temperature profile. In comparison to the packed powder bed the monolith wall showed a broader temperature distribution due to limited contact with the quartz reactor. This had an influence on the light-off behaviour because some parts of the washcoat exhibited a higher temperature where the catalyst could already ignite. This investigation emphasizes the importance of sufficient catalyst dilution and the choice of heating method in combination with the reasonable choice of the catalyst form and reactor geometry for *operando* experiments. For coatings, the possibility of integrated resistive heating may overcome the limitation of inhomogeneous temperature profiles, ensuring an optimal usage of the noble metal.

At last, the gas phase distribution during CO oxidation was investigated in a spatially resolved manner. Due to the gas sampling method, which introduces a sampling capillary through the catalyst, the WHSV within the probed channel of the monolith decreased which led to an overestimation of the catalytic activity. This was revealed by a direct comparison to a packed powder bed, containing the same amount of platinum. In the kinetic regime at 99 °C where the comparison was conducted, both catalysts were not subject to mass transfer limitations. Therefore, spatially resolved gas phase investigations should either be conducted on packed beds in order to obtain realistic gas flow profiles, or obtained by non-invasive techniques like *e.g.* planar laser induced fluorescence.

## Data availability

The data of this publication are available in the ESI† and on KITopen under the following DOI: **https://doi.org/10.35097/urp37a5c07yzeeds**

## Author contributions

S. S. planned and carried out the IR, XAS and spatially gas phase measurements, performed the data evaluation, estimated the dimensionless numbers and wrote the paper. T. D. performed the coating and the monolith wall preparation, helped during data collection and the estimation of the dimensionless numbers. F. M. helped with planing and the discussion of the results. D. S. G. supported the beamtime by building up the setup and participating in the measurements. S.-L. H. and L. K. helped with the gas phase profiling reactor. J. C. synthesized the catalyst and helped the estimation of the dimensionless numbers. A. Z. supported the conceptualization, helped with the beamtime planning as well as with the IR and XAS data evaluation and co-wrote the paper. J.-D. G. designed the study, contributed to the discussion and the interpretation of the results and co-wrote the paper.

## Conflicts of interest

There are no conflicts to declare.

## Acknowledgements

The authors would like to acknowledge the support of the Deutsche Forschungsgemeinschaft (DFG, German Research Foundation) – SFB 1441 – Project-ID 426888090. We furthermore want to thank Dr. Carina Maliakkal (Institute of Nanotechnology, KIT) and the Karlsruhe Nano Micro Facility, a Helmholtz Research Infrastructure at KIT for TEM measurements, Dr. Thomas Bergfeldt (Institute of Applied Materialscience, KIT) for ICP-OES measurements, Dr. Nicolae Barsan (Eberhard Karls University of Tübingen) for providing us the chip for the XAS investigation and Dr. Kevin Keller (ITCP, KIT) for discussion. The authors would like to thank the Institute for Beam Physics and Technology (IBPT) for the operation of the storage ring, the Karlsruhe Research Accelerator (KARA) and the KIT Light Source for the provision of X-rays at the CAT-ACT beamline. The authors thank DAPHNE4NFDI (DFG project under project number 460248799) as well as further NFDI-consortia (NFDI4Cat, FAIRMAT and NFDI4Chem) for the fruitful discussion and valuable input for implementing FAIR data principles in this work. Finally, we want to thank Dr. Matthias Hettel (ITCP, KIT) for his input on the calculation of the dimensionless numbers and Dr. Daria Gashnikova and Shweta Sharma (both ITCP, KIT) for joining the beamtime.

## Notes and references

1 A. Hart, *Biomass Convers. Biorefin.*, 2023, **13**, 11483–11498.
2 C. J. Wrasman, A. N. Wilson, O. D. Mante, K. Iisa, A. Dutta, M. S. Talmadge, D. C. Dayton, S. Uppili, M. J. Watson and X. Xu, *et al.*, *Nat. Catal.*, 2023, **6**, 563–573.
3 M. A. Bañares and M. Daturi, *Catal. Today*, 2023, **423**, 114255.
4 I. Chorkendorff and J. W. Niemantsverdriet, *Concepts of Modern Catalysis and Kinetics*, John Wiley & Sons, Weinheim, 2017.
5 J. Becher, D. F. Sanchez, D. E. Doronkin, D. Zengel, D. M. Meira, S. Pascarelli, J.-D. Grunwaldt and T. L. Sheppard, *Nat. Catal.*, 2021, **4**, 46–53.
6 J. Chen, *Ind. Eng. Chem. Res.*, 2023, **62**, 19972–19986.
7 A. Donazzi, A. Beretta, G. Groppi and P. Forzatti, *J. Catal.*, 2008, **255**, 241–258.
8 E. Tronconi, G. Groppi and C. G. Visconti, *Curr. Opin. Chem. Eng.*, 2014, **5**, 55–67.
9 B. Wollak, D. Doronkin, D. Espinoza, T. Sheppard, O. Korup, M. Schmidt, S. Alizadefanaloo, F. Rosowski, C. Schroer and J.-D. Grunwaldt, *et al.*, *J. Catal.*, 2022, **408**, 372–387.
10 C. Hess, *Chem. Soc. Rev.*, 2021, **50**, 3519–3564.
11 B. Kucharczyk and W. Tylus, *Catal. Today*, 2008, **137**, 324–328.
12 S. B. Rasmussen, R. López-Medina, R. Portela, E. Mikolajska, M. Daturi, P. Ávila and M. A. Bañares, *Catal. Sci. Technol.*, 2015, **5**, 4942–4945.
13 S. B. Rasmussen, R. Portela, P. Bazin, P. Ávila, M. A. Bañares and M. Daturi, *Appl. Catal., B*, 2018, **224**, 109–115.
14 A. Stierle, J. Gustafson and E. Lundgren, *Operando Research in Heterogeneous Catalysis*, 2017, pp. 59–87.
15 S. W. Chee, T. Lunkenbein, R. Schlögl and B. Roldan Cuenya, *J. Phys.: Condens. Matter*, 2021, **33**, 153001.
16 J.-D. Grunwaldt and B. S. Clausen, *Top. Catal.*, 2002, **18**, 37–43.
17 B. Torkashvand, L. Maier, P. Lott, T. Schedlbauer, J.-D. Grunwaldt and O. Deutschmann, *Top. Catal.*, 2019, **62**, 206–213.
18 S. Wan, T. Häber, P. Lott, R. Suntz and O. Deutschmann, *Appl. Energy Combust. Sci.*, 2023, **16**, 100229.
19 A. Zellner, R. Suntz and O. Deutschmann, *Angew. Chem., Int. Ed.*, 2015, **54**, 2653–2655.
20 J. Rotta, *Arch. Appl. Mech.*, 1956, **24**, 258–281.
21 D. E. Doronkin, H. Lichtenberg and J.-D. Grunwaldt, in *XAFS Techniques for Catalysts, Nanomaterials, and Surfaces*, ed. Y. Iwasawa, K. Asakura and M. Tada, Springer, Berlin, 1st edn, 2017, ch. Cell Designs for In Situ and Oerando Studies, pp. 75–89.
22 H. Bai, J. Theuerkauf, P. A. Gillis and P. M. Witt, *Ind. Eng. Chem. Res.*, 2009, **48**, 4060–4074.
23 A. Jafari, P. Zamankhan, S. Mousavi and K. Pietarinen, *Chem. Eng. J.*, 2008, **144**, 476–482.
24 A. H. Thaker, G. Karthik and V. V. Buwa, *Chem. Eng. J.*, 2019, **374**, 189–200.
25 X. Guo and R. Dai, *Particuology*, 2010, **8**, 293–299.
26 F. Maurer, A. Gänzler, P. Lott, B. Betz, M. Votsmeier, S. Loridant, P. Vernoux, V. Murzin, B. Bornmann, R. Frahm, O. Deutschmann, M. Casapu and J.-D. Grunwaldt, *Ind. Eng. Chem. Res.*, 2021, **60**, 6662–6675.
27 A. Donazzi, D. Livio, A. Beretta, G. Groppi and P. Forzatti, *Appl. Catal., A*, 2011, **402**, 41–49.
28 H. Li, M. Rivallan, F. Thibault-Starzyk, A. Travert and F. C. Meunier, *Phys. Chem. Chem. Phys.*, 2013, **15**, 7321–7327.
29 M. Hettel, C. Diehm, B. Torkashvand and O. Deutschmann, *Catal. Today*, 2013, **216**, 2–10.
30 D. Livio, C. Diehm, A. Donazzi, A. Beretta and O. Deutschmann, *Appl. Catal., A*, 2013, **467**, 530–541.
31 R. Horn, O. Korup, M. Geske, U. Zavyalova, I. Oprea and R. Schlögl, *Rev. Sci. Instrum.*, 2010, **81**, 064102.
32 L. Klag, S. Weber, R. Horn, T. L. Sheppard and J.-D. Grunwaldt, *Catal. Sci. Technol.*, 2024, 863–877.
33 D. Espinoza, B. Wollak, T. L. Sheppard, A.-C. Dippel, M. Sturm, O. Gutowski, M. Schmidt, O. Korup and R. Horn, *ChemCatChem*, 2022, **14**, e202200337.
34 V. Berg, M. Geske, O. Korup, M. Schmidt, F. Rosowski, A. Karpov, M. Kraemer and R. Horn, *Ind. Eng. Chem. Res.*, 2024, 3891–3909.
35 W. Kleist and J.-D. Grunwaldt, in *Modern Applications of High Throughput R&D in Heterogeneous Catalysis*, ed. A. Hagemeyer and A. F. Volpe Jr, Bentham Science Publishers, Sharjah, 1st edn, 2014, ch. High Outut Catalyst Development in Heterogeneous Gas Phase Catalysis, pp. 354–358.
36 S. Müller, A. Zimina, R. Steininger, S. Flessau, J. Osswald and J.-D. Grunwaldt, *ACS Sens.*, 2020, **5**, 2486–2496.

37 A. Zimina, K. Dardenne, M. A. Denecke, D. E. Doronkin, E. Huttel, H. Lichtenberg, S. Mangold, T. Pruessmann, J. Rothe, T. Spangenberg, R. Steininger, T. Vitova, H. Geckeis and J.-D. Grunwaldt, *Rev. Sci. Instrum.*, 2017, **88**, 113113.
38 B. Ravel and M. Newville, *J. Synchrotron Radiat.*, 2005, **12**, 537–541.
39 E. Golubina, T. Rostovshchikova, E. Lokteva, K. Maslakov, S. Nikolaev, M. Shilina, S. Gurevich, V. Kozhevin, D. Yavsin and E. Slavinskaya, *Appl. Surf. Sci.*, 2021, **536**, 147656.
40 J. Pérez-Ramırez, R. J. Berger, G. Mul, F. Kapteijn and J. A. Moulijn, *Catal. Today*, 2000, **60**, 93–109.
41 M. Baerns, *Technische Chemie*, John Wiley & Sons, Weinheim, 2013.
42 G. F. Froment, K. B. Bischoff and J. De Wilde, *Chemical reactor analysis and design*, John Wiley & Sons, New York-Chichester, 3rd edn, 2010, pp. 186–195.
43 D. Seguin, A. Montillet, J. Comiti and F. Huet, *Chem. Eng. Sci.*, 1998, **53**, 3897–3909.
44 R. Pečinka, M. Blažek, R. Knopp, P. Kočí and A. York, *Chem. Eng. Sci.*, 2022, **260**, 117876.
45 B. Torkashvand, L. Maier, M. Hettel, T. Schedlbauer, J.-D. Grunwaldt and O. Deutschmann, *Chem. Eng. Sci.*, 2019, **195**, 841–850.
46 F. U. Renner, A. Stierle, H. Dosch, D. M. Kolb, T.-L. Lee and J. Zegenhagen, *Phys. Rev. B: Condens. Matter*, 2008, **77**, 235433.
47 M. Plodinec, H. C. Nerl, R. Farra, M. G. Willinger, E. Stotz, R. Schlögl and T. Lunkenbein, *Microsc. Microanal.*, 2020, **26**, 220–228.
48 F. Tao, *ChemCatChem*, 2012, **4**, 583–590.
49 A. M. Gänzler, M. Casapu, D. E. Doronkin, F. Maurer, P. Lott, P. Glatzel, M. Votsmeier, O. Deutschmann and J.-D. Grunwaldt, *J. Phys. Chem. Lett.*, 2019, **10**, 7698–7705.
50 J.-D. Grunwaldt, M. Caravati, S. Hannemann and A. Baiker, *Phys. Chem. Chem. Phys.*, 2004, **6**, 3037–3047.
51 I. Langmuir, *Trans. Faraday Soc.*, 1922, **17**, 621–654.
52 E. Alayon, J. Singh, M. Nachtegaal, M. Harfouche and J. A. van Bokhoven, *J. Phys.: Conf. Ser.*, 2009, **190**, 012152.
53 G. Bunker, *Introduction to XAFS: a practical guide to X-ray absorption fine structure spectroscopy*, Cambridge University Press, 2010.
54 S. Wang, C. Xu, W. Liu and Z. Liu, *Energies*, 2019, **12**, 414.
55 D. Eggart, A. Zimina, G. Cavusoglu, M. Casapu, D. E. Doronkin, K. A. Lomachenko and J.-D. Grunwaldt, *Rev. Sci. Instrum.*, 2021, **92**, 023106.
56 S. Ceylan, L. Coutable, J. Wegner and A. Kirschning, *Chem. – Eur. J.*, 2011, **17**, 1884–1893.
57 W. Wang, G. Tuci, C. Duong-Viet, Y. Liu, A. Rossin, L. Luconi, J.-M. Nhut, L. Nguyen-Dinh, C. Pham-Huu and G. Giambastiani, *ACS Catal.*, 2019, **9**, 7921–7935.
58 M. Hettel, C. Antinori and O. Deutschmann, *Emiss. Control Sci. Technol.*, 2016, **2**, 188–203.
59 M.-A. Serrer, M. Stehle, M. L. Schulte, H. Besser, W. Pfleging, E. Saraçi and J.-D. Grunwaldt, *ChemCatChem*, 2021, **13**, 3010–3020.